RSC Advances

PAPER

View Article Online
View Journal | View Issue

Cite this: *RSC Adv.*, 2023, **13**, 3635

Dramatic improvement in the mechanical properties of polydopamine/polyacrylamide hydrogel mediated human amniotic membrane

Lin Peng,[a] Yufei Liang,[b] Jianling Yue,[b] Hanmei Li,[a] Aimin Deng,[a] Shun Xie,[a] Xiu-Zhi Tang,[c] Jing Wang *[d] and Zenghui Mao*[a]

Received 30th November 2022
Accepted 17th January 2023

DOI: 10.1039/d2ra07622e

rsc.li/rsc-advances

Human amniotic membrane (hAM) is a promising material for tissue engineering due to several benefits, including desirable biocompatibility, stem cell source, antibacterial activity, *etc*. However, because of its low elasticity, the clinical application of hAM is severely restricted. To solve this issue, we employed polydopamine/polyacrylamide (PDA/PAM) hydrogels to toughen hAM. The test results indicated that the PDA/PAM hydrogel can enhance the toughness of hAM dramatically due to the formation of abundant chemical bonds and the strong mechanical properties of the hydrogel itself. Compared to pure hAM, the break elongation and tensile strength of PDA/PAM-toughened hAM rose by 154.15 and 492.31%, respectively. And most importantly, the fracture toughness was almost 15 times higher than untreated hAM. In addition, the cytotoxicity of the PDA/PAM-coated hAM was not detected due to the superior biocompatibility of the chemicals used in the study. Treating hAM with adhesive hydrogels to increase its mechanical characteristics will further promote the application of hAM as a tissue engineering material.

1 Introduction

The prevalence of intrauterine adhesions, a troublesome gynecological disease that poses a significant risk to women's reproductive health, is one of the most pressing issues facing gynecologists today.[1–5] Human amniotic membrane (hAM) is an ideal material with great potential to prevent postoperative adhesion because of its natural biocompatibility and unique properties, such as self-contained stem cells, antibacterial properties, and flexibility. Clinical studies have demonstrated that hAM can treat moderate and severe intrauterine adhesions with specific feasibility and safety benefits, as the stem cells in hAM could effectively promote the repair of endometriosis.[6–9] Furthermore, treating intrauterine adhesions with hAM can restore the self-repairing ability of the endometrium and restore the normal menstrual and reproductive functions of women.[10–14] However, the mechanical properties, particularly the tensile property of the hAMs used in surgeries, are insufficient, severely restricting the promotion and application of hAMs.[15–18]

Hydrogel is a material that contains a large amount of water in an internal three-dimensional network, and it has similar physical and biological properties to the extracellular matrix, making it an ideal bioadhesive material for various tissues.[19–26] Hydrogels' superior adhesion, biocompatibility, degradation, and antibacterial properties have led to rapid advancements in the field of bioadhesion in recent years.[27] Hydrogel's adjustable adhesion strength and designed surface chemical group make it applicable in various substrates, and the biocompatibility of the hydrogel can prevent negative effects on the body, which is expected to enhance the further development of hydrogel in the biomedical field.[28–30] Combining high-toughness adhesive hydrogel with hAM by optimizing the interface is supposed to improve the mechanical properties of hAM and maintain the biocompatibility of hAM.[27,31–34]

In recent years, with the in-depth study of the natural bioadhesion mechanism, many biomimetic adhesion surfaces have been designed to solve problems such as wet tissue adhesion, which provides a research basis for the surface adhesion and toughening of hAM. Inspired by the adhesion mechanism of mussels, scientists have studied a series of substances containing catechol groups.[35–37] Previous studies have shown that hydrogels containing catechol groups form covalent bonds, metal coordination bonds or hydrogen bonds with different materials, forming strong adhesion.[33,35,36,38–41] In principle, catechol is easily oxidized to form active quinones, which could trigger secondary reactions with macromolecules containing amino or sulfhydryl groups through Michael addition reactions or Schiff base reactions, resulting in protein

[a]*Changsha Hospital for Maternal and Child Health Care Affiliated to Hunan Normal University, Changsha 410083, China. E-mail: zhmao48@163.com*

[b]*Powder Metallurgy Research Institute, Central South University, Changsha, 410083, China*

[c]*Research Institute of Aerospace Technology, Central South University, Changsha, 410083, China*

[d]*Department of Pathology, Xiangya Hospital, Central South University, Changsha 410083, China. E-mail: wj020501@163.com*

crosslinking and tissue adhesion. Therefore, amino groups in biological tissues can react with catechol groups in hydrogels to form imine bonds at the interface.[36]

Polyacrylamide (PAM), an easy-to-fabricated and low-cost hydrogel with abundant active $-NH_2$ group, is feasible for tissue engineering due to its conformal characteristic and biocompatibility. Nevertheless, the pure PAM is usually brittle and weak when suffering from external tensile strain because of the low crosslinking points and weak interaction among polymer chains. Therefore, the poor stretchability of PAM makes it hard to meet the essential requirement of adhesion for most soft tissues. Previous works have confirmed that incorporating polydopamine (PDA, containing abundant catechol groups) into PAM chains could improve the mechanical and adhesive performances of PDA/PAM hydrogel remarkably.[42–45] The highly ductile PDA/PAM hydrogel exhibits excellent self-healing ability, strong cell affinity and desirable wound closure.[46] Whereas the application environment for the PDA/PAM hydrogel in Lu's work is restricted to *in vitro* skin, which is distinctly different from the soft and wet tissue such as hAM. Traditional hydrogels typically have weak adhesion to moisture and flexible biological tissues.[47,48] Hydrogels have poor surface energy and adhesion strength because the high water content of the matrix prevents the hydrogels from making direct contact with the substrates.[48] Consequently, it is clinically significant to design and fabricate a bioadhesive material that can firmly adhere to wet tissues to prevent tissue adhesion.[48–51] Despite the PDA/PAM and its derivative being exploited for tissue engineering, the previous works mainly focused on the function of hydrogels themselves. However, the capacity of adhesive hydrogels to endow substrates with improved stretchability has failed to demonstrate, which is vital to the application of hAM.

Therefore, in this work, PDA/PAM hydrogel is fabricated and adhered to hAM. Due to the introduction of PDA increasing the number of hydrophilic groups, the swelling performance was improved accordingly. Moreover, more hydrogen bonds between hydrogels and substrates enhance the adhesion strength compared to pure PAM. For the mechanical property, as compared to the unmodified PAM, the PDA/PAM-toughened hAMs have more than twice the elongation at break and tensile strength. In particular, the fracture toughness is about 10 times higher than the hAM. Because of the elaborately selected chemicals for the fabrication of PDA/PAM, the treated hAM has no cytotoxicity.

2 Results and discussion

In the experiment of preparing PDA/PAM hydrogel, dopamine will be oxidized, and catechol on the benzene ring will be oxidized to benzoquinone in an aerobic alkaline environment. After the self-polymerization, the polydopamine was successfully obtained and the solution gradually changed from colorless to brown, thus forming the first hydrogel network. After introducing PAM networks, the phenolic hydroxyl groups of polydopamine interact with the amino groups of acrylamide *via* covalent bonds or hydrogen bonds; meanwhile, the oxidized benzoquinone also reacts with the amino groups by a Schiff base reaction. Thus, the PDA/PAM double network hydrogel can be obtained, as shown in Fig. 1.

Similarly, in the experiment of toughening amniotic membrane with PDA/PAM hydrogel (Fig. 2), the Schiff base reaction and Michael addition reaction are two primary reactions between hydrogel and tissue surface nucleophile (−SH, $-NH_2$). Specifically, the formed semi-benzoquinone or benzoquinone structure can react with amino groups and sulfhydryl groups on the amniotic membrane surface by Michael addition reaction or Schiff base reaction. At the same time, phenol on PDA and carbonyl on PAM can also form hydrogen bonds with amino groups, providing a non-covalent interaction and enhancing surface adhesion to tissues.

Fig. 3 is the FTIR of PDA, PAM, pure hAM and PDA/PAM-treated hAM. For the PDA, three peaks located at 1286, 1508 and 1602 ascribed to the –OH, aromatic ring and –C–N, respectively. For PAM, 1415, 1452 and 1625 corresponding to –C–N (stretching of primary amide), $-CH_2$ (in-plane scissoring) and –C–N– (primary amine) can be observed.[46] Five characteristic absorption peaks appeared in the curve of pure hAM: amide A band, amide B band, amide I band, amide II band, and amide III bands. Specifically, the absorption peak of the amide A band located at 3296 cm^{-1} belongs to the N–H characteristic vibration. And the absorption peak of the amide B band appeared at 3076 cm^{-1} is ascribed to the CH_2 asymmetric stretching vibration. While the absorption peak of the amide I band centered at 1636 cm^{-1} is the C=O stretching vibration. The collagen molecule's characteristic peak of α-helix structure is also observed from 1600 to 1700 cm^{-1}.[52,53] Since all peptide bonds in the peptide chain can form hydrogen bonds, the structure of α-helix is believed to be very stable. The absorption peak corresponding to the typical amide II band is 1541 cm^{-1} due to the C–N stretching and the N–H bending vibration.

Furthermore, the peak at 1237 cm^{-1} is caused by the N–H bending vibration. All the peaks mentioned above implies the hAM contains numerous hydrophilic groups, which is convenient for the subsequent hydrogel attachment. After being

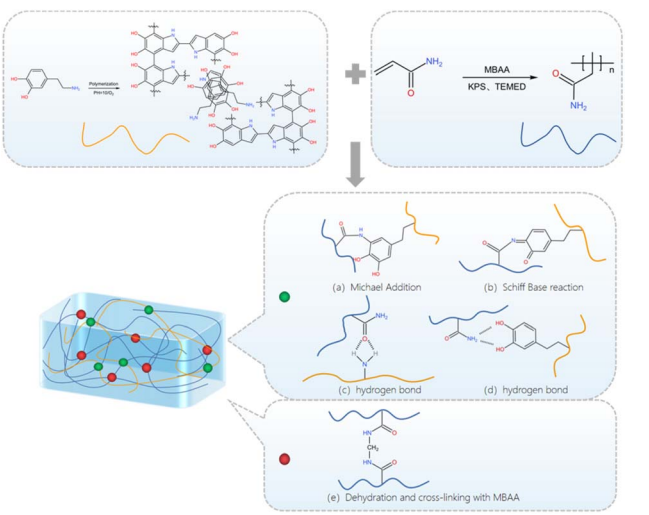

Fig. 1 Synthetic route of PDA/PAM hydrogel.

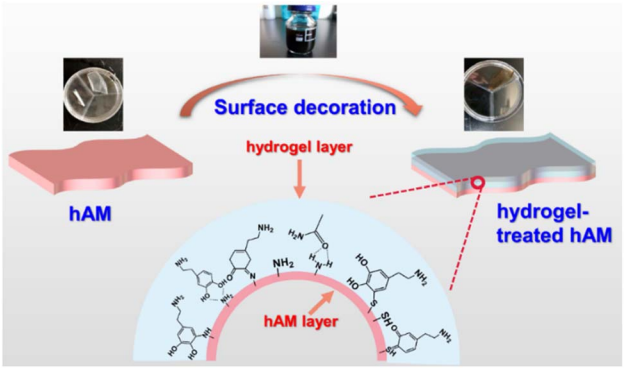

Fig. 2 Schematic illustration of hydrogel-modified hAM.

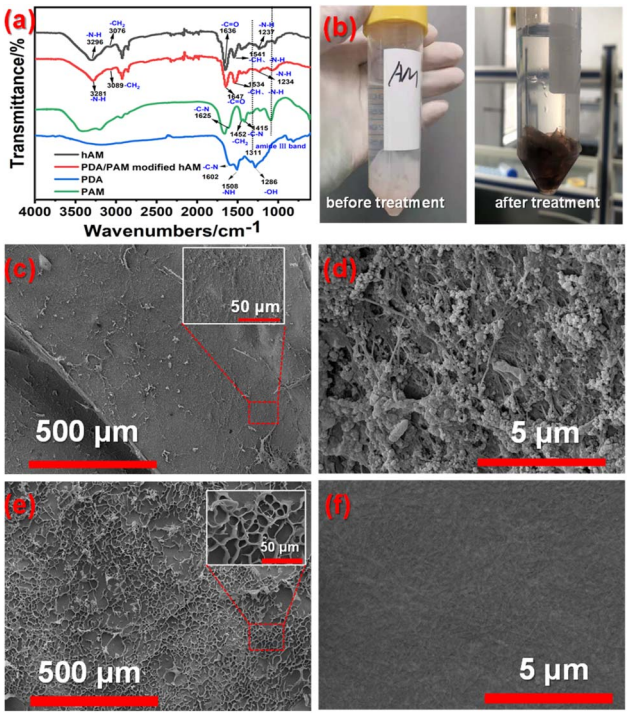

Fig. 3 (a) FTIR of hAM and PDA/PAM modified hAM; (b) digital photos of hAM before and after treatment; surface morphologies of hAM (c and d) and PDA/PAM treated hAM (e and f).

treated by PDA/PAM hydrogel, the peak of the amide A band shifted to 3281 cm^{-1}, which is lower than that of pure hAM, suggesting the strong interaction between the N–H group of collagen molecule and the C=O group of the hydrogel. Compared to the FTIR curve of hAM, there are two peaks at 1325 cm^{-1} (amide III band) and 1080 cm^{-1} (C–C asymmetric stretching) originating from PAM can be seen in the curve of hydrogel-treated hAM. Accordingly, the absorption peak of the amide B band shifts from 3076 to 3089 cm^{-1}. The absorption of the amide I band blue shifts to 1647 cm^{-1} as compared to the pure hAM, which may be caused by partial denaturation of collagen to reduce the bond length of C=O. Based on the principle of FTIR, the stretching vibration is inversely proportional to the square root of the bond length, so the typical blue shift occurred. Correspondingly, the amide II is 1534. Moreover, the photo permeability of the modified hAM samples was generally lower than that of pure hAMs due to the thicker PDA/PAM-treated hAM and the darker color (Fig. 3b).

Furthermore, the surface morphologies of as-received hAM and hydrogel-modified hAM were investigated by SEM images. As shown in Fig. 3c, the surface of freeze-dried pure hAM is rough and many holes with very thin walls formed as a result of a serious dehydration process. Observed from the insert map of Fig. 3c, many fibrous stands regarded as collagenous fibers protruded from the membrane. The flat areas without wrinkles presented in Fig. 3d are clean and smooth, but several fibrous structures can still be seen. Comparatively, for the PDA/PAM treated hAM, both Fig. 3d and partially enlarged details displayed relatively flat surfaces, due to the filled effect from the attached polymer. The further magnified image shown in Fig. 3d indicated the rough hAM surface decorated with agglomerated polymers.

The surface hydrophilicity and abundant precursor of hydrogen bonds would offer the hydrogel desirable adhesion to substrates (Fig. 4a). The test details for evaluating adhesion property were described in the experimental section, and the stress–strain curves of PAM and PDA/PAM were recorded through the lap shear test (Fig. 4b–e). As shown in Fig. 4b, the adhesion strength provided by PDA/PAM hydrogel for the glass substrate is 7.73 Pa, much higher than 4.8 Pa of PAM hydrogel. When the substrate was changed to the typical plastic material, for example, a PET board, we found the adhesion strength of PET-PDA/PAM fell to 2.55 Pa, which is still higher than PET-PAM of 0.68 Pa (Fig. 4c). In comparison, the adhesive strength of PDA/PAM to pig skin is calculated to be 6.14 Pa (Fig. 4d), while PAM hydrogel cannot adhere to pigskin at all. The experimental results show that PDA/PAM hydrogel exhibits broad adhesion towards glass plate (inorganic material), PET plate (organic material) and pigskin (biological material). Moreover, compared to pure PAM hydrogel, PDA/PAM hydrogel shows stronger adhesive strength, suggesting that

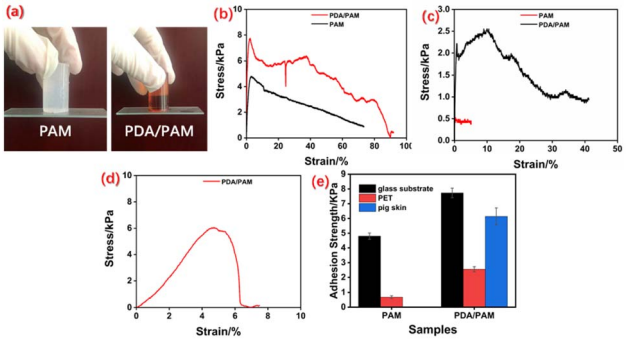

Fig. 4 Adhesion state of PAM and PDA/PAM toward the glass substrate (a); peel curves of PAM and PDA/PAM hydrogel attached on glass (b), polyethylene terephthalate (PET) (c) and pig skin (d); adhesion strength of PAM and PDA/PAM on glass substrate, PET and pig skin (e).

incorporating PDA can effectively improve the interaction between hydrogel and substrate.

The adhesive hydrogel is supposed to be the ideal toughening material for the weak hAM, and its intrinsic mechanical property plays a vital role in the final toughness performance. Fig. 5a shows that the neat PAM hydrogel can be stretched from an initial 5 cm to a breaking length of 9.5 cm with a corresponding elongation of 90%. While the PDA/PAM hydrogel can be stretched from 3 cm to 8 cm (Fig. 5b) and realize a further improved elongation of 166%, indicating the introduction of PDA can improve the tensile property of hydrogel significantly. As shown in Fig. 5c–d, in addition to the elongation, the tensile strength values of PAM and PDA/PAM hydrogel are 0.026 and 0.084 M076Pa, respectively. This is because the added DA is readily oxidized under the alkaline condition to generate active dopaquinone groups. These active groups could further self-polymerize or react with $-NH_2$ *via* Michael addition or Schiff base reaction, thereby forming a crosslinked and dual network structure between PDA and PAM chains. Moreover, many physical crosslinking points generate *via* π–π interactions or hydrogen bonds due to the catechol group from polydopamine and $-NH_2$ groups from PAM. In principle, the interlocked structure and the intensive hydrogen bonds in the hydrogel could dissipate external stress and increase the stretch property during the deformation.

The hAM has excellent potential in tissue engineering due to its superior biocompatibility and abundant stem cells. However, the poor mechanical performance, especially for its tensile property, has severely impeded the further application of the hAM.[54–57] Fig. 6a shows the toughening effect of hAMs modified by PDA/PAM. According to the calculated results (Fig. 6b), the elongation at break, the tensile strength, and the fracture toughness of pure hAM are 24.10%, 0.13 MPa, and 1.25 MPa $m^{1/2}$, respectively. In striking contrast, the elongation at break, the tensile strength, and the fracture toughness of the PDA/PAM hydrogel toughened hAM rise to 61.25%, 0.77 MPa, and 18.39 MPa $m^{1/2}$, respectively. Therefore, the elongation at break and the tensile strength increased by 154.15% and 492.31%, respectively, compared to pure hAM. Notably, the fracture toughness is about 15 times higher than the as-received hAM. The above results demonstrate that the PDA/PAM hydrogel has a remarkable toughening effect on the tensile property of the hAM.

As the application environment of hydrogel is usually wet, the swelling property of hydrogel must be investigated.

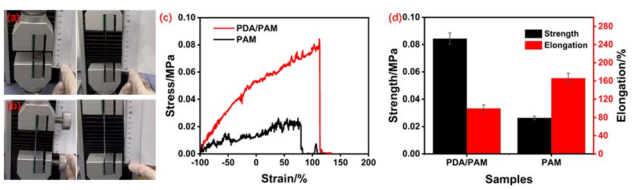

Fig. 5 Initial and fracture stage of PAM (a) and PDA/PAM upon stretching (b); stress–stain curves of PAM and PDA/PAM (c); tensile strength and elongation of PAM and PDA/PAM (d).

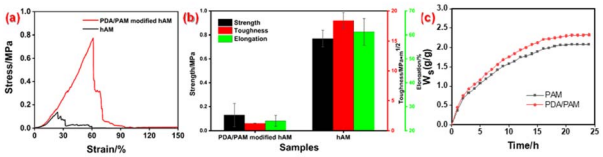

Fig. 6 Tensile curves (a), mechanical performances of (b) and swelling performances of hAM and PDA/PAM modified hAM (c).

According to the swelling curves plotted in Fig. 6c, the swelling rate of the hydrogel is very fast in the first few hours, and then the increase of the mass decerebrated remarkably. Finally, the typical plateau appears for all curves because the absorption and release of water reach a dynamic equilibrium. Throughout the whole swelling procedure, the W_s value of PDA/PAM hydrogel is higher than that of PAM. This phenomenon can be explained by the more crosslinking points and hydrophilic groups, leading to the enhanced absorption capacity and maintaining the capacity of water in the dual network of PDA/PAM.

Fig. 7a and b shows the rheological performances of PAM hydrogel and PDA/PAM hydrogel tested under condition 1. The storage modulus G' and loss modulus G'' of PAM together with the G'' of PDA/PAM decrease with the increase of strain, indicating that the intermolecular association of the polymer is unstable and can be destroyed under high strain. Nevertheless, the G' of the PDA/PAM is higher than that of PAM and decreases more slowly, implying the intermolecular association structure of PDA/PAM hydrogel is more stable than that of PAM hydrogel. Fig. 7c and d shows the rheological curve of PAM hydrogel and PDA/PAM hydrogel recorded under condition 2. In the scanning frequency range of 0.1–100 Hz, the G' for both PAM and PDA/PAM increases with frequency, while the G'' decreases. This is because the polymer molecules are relaxed at a low frequency and the intermolecular association is weak. Thus, most of the

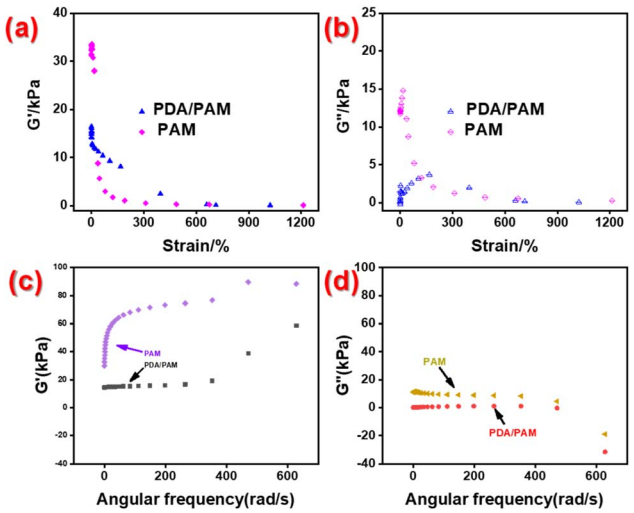

Fig. 7 Rheological properties of PAM and PDA/PAM test under condition 1 (a and b) and 2 (c and d).

energy is released through viscous flow. Nonetheless, as the frequency of interactions increases, some intramolecular associations are broken to form intermolecular associations and increase the number of intermolecular entanglement points. The crosslinked state produced may increase G' and decrease G''. Moreover, the G' of PDA/PAM hydrogels is significantly lower than that of PAM, which is a common occurrence in hydrogels containing PDA due to its inhibitory effect on free radical polymerization.[58] Nevertheless, the storage modulus G' of the PDA/PAM hydrogel is still larger than the loss modulus G'', indicating the superior rheological property of dual network hydrogel.

The cytotoxicity is necessary and critical for the practical application of modified hAMs. Fortunately, the results in Fig. 8 confirm that the absorbances of the (DMEM/F12 + 10% FBS + bFGF) and (extraction solution + 10% FBS + bFGF) groups were 0.67 and 0.78 ($p < 0.05$, $n = 5$), respectively. Since the absorbance of the (DMEM/F12 + 10% FBS + bFGF) is lower than that of the (extraction solution + 10% FBS + bFGF) group, the number of living cells in the extractions solution of hydrogel-modified hAM increased rather than decreased. The increased cell number demonstrates the extraction solution provides a more profitable environment for cell proliferation, suggesting the modified hAM has no cytotoxicity.

3 Conclusions

In summary, a dual network hydrogel incorporated PDA with PAM was fabricated and successfully attached to the hAM. The addition of PDA increases the hydrophilic groups and promotes the formation of hydrogen bonds between hydrogels and substrates. Therefore, PDA/PAM hydrogel shows better adhesion ability towards PET board, glass plate and pigskin than pure PAM. The mechanical property of PDA/PAM is also superior to PAM because of the crosslinked and dual network structure. The elongation at break and tensile strength of PDA/PAM toughened hAMs are enhanced dramatically. Notably, the fracture toughness of PDA/PAM-modified hAM is approximately 15 times greater than the as-received hAM. Owing to the more crosslinking points and hydrophilic groups, compared with PAM hydrogels, the PDA/PAM hydrogel shows a remarkably improved mechanical behavior and more stable rheological property after adding dopamine. In conclusion, this study on the PDA/PAM hydrogel provides a new idea for the toughening hAM and broadens the application scope of hAM in biomedicine.

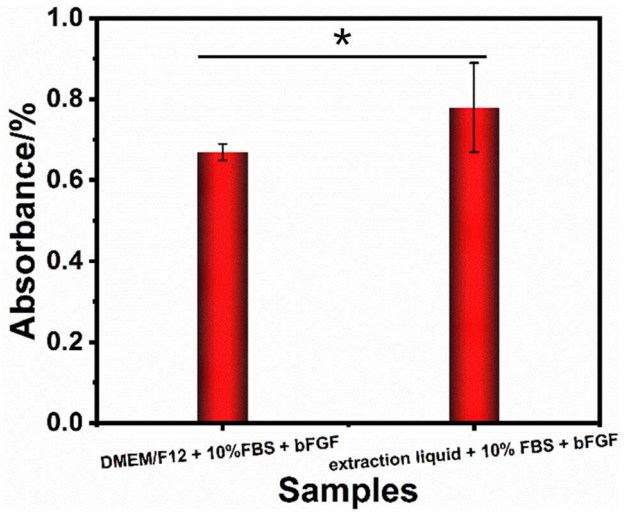

Fig. 8 The cytotoxicity results of the extraction liquid for the PDA/PAM treated hAM and a corresponding blank group, *$p < 0.05$.

4 Experimental

4.1 Materials

Fatal Bovine serum (FBS, Gibco), CellTiter 96® AQueous One Solution Cell Proliferation Assay(a) (Sigma), 3-(4,5-diethylthiazol-2-yl)-5-(3-carboxymethoxy-phenyl)-2-(4-sulfophenyl)-2*H*-etrazolium, inner salt (MTS), Dulbecco's Modified Eagle Medium/F12(DMEM/F12,Gibco) and Basic Fibroblast Growth Factor (bFGF, Sigma) were used without further processing. Dopamine hydrochloride (DA), *N,N*′-methylene diacrylamide (MBA), tetramethyl ethylenediamine (TEMED) and sodium hydroxide (sheet) were purchased from Shanghai Aladdin Biochemical Technology Co., Ltd, China. Acrylamide (AM), ammonium persulfate (APS) and potassium persulfate (KPS) were provided by National Pharmaceutical Group Corporation, China. Normal saline was commercially obtained from Renhua Pharmaceutical Group Co. LTD, China. All the chemicals were analytical grade and were used without further purification. All aqueous solutions were bubbled under nitrogen for more than 30 minutes.

4.2 Preparation of polyacrylamide (PAM) hydrogel

Acrylamide (AM, 2.5 g) was placed into a beaker and mixed with 1 mL of APS solution (0.0038 g mL^{-1}). After that, more deionized water was supplemented until the volume reached 10 mL. Subsequently, 2 μL tetramethylethylenediamine (TEMED) as the co-initiator was added and sonicated for 2 minutes. The polymer precursor solution was slowly poured into the mold, and the polymerization was carried out in a refrigerator at 4 °C to suppress bubble formation. When the hydrogel was formed, the mold was taken out and the reaction was continued for another 4 days to produce the pure PAM hydrogel.

4.3 Preparation of PDA/PAM hydrogel

Firstly, 3.75 mg dopamine hydrochloride (DA) was dissolved in 15 mL NaOH aqueous solution (pH ~ 9) under a 20 min stir. Then, 2.5 g AM and 20 mg cross-linker *N,N*′-methylenebisacrylamide (MBAA) were added and sonicated until the solids were dissolved. Afterwards, the initiator potassium persulfate (KPS, 200 mg) and 10 μL co-initiator TEMED was introduced. Subsequently, PDA/PAM hydrogel polymerization was operated according to the same steps as the fabrication of PAM hydrogel. Finally, a yellow-brown PDA/PAM hydrogel was obtained.

4.4 Fabrication of PDA/PAM hydrogel toughened hAM

Firstly, a piece of pretreated AM with a size of 5 cm × 5 cm was soaked in 50 mL saline solution, the pH value of which was adjusted to 9–10 with 0.1 mol L^{-1} NaOH solution. Afterwards, 100 mg DA was dissolved in the alkaline saline solution *via* sonication. After being stirred for 40 minutes at a speed of 200 r/min, 1 g AM, 0.5 mL KPS (0.0038 g mL^{-1}) and 2 μL TEMED were added to the solution, and the reaction was carried out for 2 hours under mild stirring. Finally, a piece of hAM treated by PDA/PAM hydrogel was obtained.

4.5 Tensile test

The tensile properties of the prepared hydrogel and film samples were tested by a universal tensile testing machine (WBE-9010B) from Dongguan Weibang Instrument Equipment Co., Ltd. The hydrogel was cast into typical dumbbell-shaped test strips with a size of 10 mm × 75 mm × 3 mm. For the hAM and modified hAM, the samples were cut down into the geometry with a length of 50 mm and a width of 40 mm according to the method proposed by Koh *et al.*[59] The crosshead speed was 40 mm min^{-1}. All tensile tests were performed under room conditions.

4.6 Adhesion performance test

The adhesive performance of various hydrogels was measured using a universal testing machine (Instron 5567). The hydrogels with the dimension of 10 mm × 50 mm × 2 mm were sandwiched between glass plates, stainless steel plates, and pigskin, respectively. The surface of fresh pig skins was cleaned to remove liquids and grease before testing. The contact area (S) between the hydrogel and the adherend is 500 mm^2. All tests were carried out at room temperature with a tensile speed of 10 mm min^{-1}, and the adhesion value (P) was given by

$$P(\mathrm{Pa}) = F(\mathrm{N})/S(\mathrm{m}^2)$$

where F is the force when the hydrogel is torn off.

4.7 Swelling performance test

The hydrogels were soaked in distilled water at room temperature and taken out every other hour. Before weighting, the absorbed water on the surface of hydrogels was removed entirely. The hydrogel swelling degree (W_s, %) was calculated according to the following formula:

$$W_s = (m_1 - m_0)/m_0 \times 100\%$$

where m_1 is the weight of the soaked hydrogels, and m_0 is the initial weight of the hydrogels.

4.8 Rheological property

The hydrogel was processed into a cylindrical shape with a diameter of 25 mm and a thickness of 5 mm before placing on a rotational rheometer (Physical MCR301, MCR50). The test was operated based on the following two conditions: (1) the normal force was set as 20 N, the sweep frequency was fixed at 1 rad s^{-1}, and the strain ranged from 0.1% to 1000%; (2) the strain was 1% strain, and sweep frequency is in the range of 0.1–100 Hz.

4.9 Cells toxicity test

4.9.1 Toughening amniotic membrane extraction fluid collection. As-synthetic hAM was soaked in DMEM/F12 (the basal medium used for cell culture) for 48 hours. Then the soaking liquid (extract) was collected and filtered by a 0.22 μm sterile needle filter. The extraction liquid was stored at 4–7 °C for one week.

4.9.2 Cytotoxicity test. MTS assay was used to detect cell viability and evaluate the cytotoxicity of toughened amniotic membrane. P2 human umbilical cord mesenchymal stem cells (hUMSCs) were seeded into 96-well plates at a density of 2×10^3 cells per well and cultured overnight. When the cells were attached to the wall, they were replaced with the following medium: DMEM/F12 + 10% FBS + bFGF (10 ng mL^{-1}), extraction liquid + 10% FBS + bFGF (10 ng mL^{-1}), and blank wells (DMEM/F12 and extraction liquid were added, respectively). 100 μL medium was added to every well. Then, the 96-well plates were incubated at 37 °C, 5% CO_2 for 24 hours, 20 μL MTS was added to each well. After 3 hours of incubation, the absorbance value of each well was detected by an enzyme-linked immunodetection at 490 nm wavelength. The study was approved by the Ethics Committee of Changsha Hospital for Maternal and Child Health Care in China (No. 2022014).

Author contributions

J. W. and Z. M. conceived and designed this work. L. P., Y. L. and H. L. performed the experiments. J. Y., A. D. and S. X. discussed the results and participated in the preparation of the paper. J. W. and X. T. wrote the manuscript.

Conflicts of interest

The authors declare no competing financial interest.

Acknowledgements

This research was financially supported by Health Commission of Hunan Province (No. 202202054141).

References

1 M. N. Collins and C. Birkinshaw, *Carbohydr. Polym.*, 2013, **92**, 1262–1279.
2 G. F. Grimbizis, A. D. S. Sardo and R. Campo, *Fertil. Steril.*, 2021, **116**, 1188.
3 J. Wang, C. Yang, Y. Xie, X. Chen, T. Jiang, J. Tian, S. Hu and Y. Lu, *Front. Bioeng. Biotechnol.*, 2021, **9**, 760943.
4 D. Zhang, C. Ding, T. Duan and Q. Zhou, *Front. Mater.*, 2022, **9**, 942957.
5 X. Zhang, G. Chen, Y. Wang, L. Fan and Y. Zhao, *Adv. Sci.*, 2022, **9**(12), 2104883.

6 L. Echarte, G. Grazioli, L. Pereira, A. Francia, H. Perez, W. Kuzuian, W. Vicentino, H. Pardo, A. Mombru, A. Maglia, C. Tourino and I. Alvarez, *Cell Tissue Banking*, 2022, DOI: 10.1007/s10561-022-10014-8.
7 M. Fenelon, S. Catros, C. Meyer, J.-C. Fricain, L. Obert, F. Auber, A. Louvrier and F. Gindraux, *Membranes*, 2021, **11**(6), 387.
8 A. Gremare, L. Thibes, M. Gluais, Y. Torres, D. Potart, N. Da Silva, N. Dusserre, M. Fenelon, L. Sentilhes, S. Lacomme, I. Svahn, E. Gontier, J.-C. Fricain and N. L'Heureux, *Biofabrication*, 2022, **14**, 045010.
9 J. Zhao, M. Tian, Y. Li, W. Su and T. Fan, *Acta Biomater.*, 2022, **147**, 185–197.
10 G. Cai, Z. Hou, W. Sun, P. Li, J. Zhang, L. Yang and J. Chen, *Front. Bioeng. Biotechnol.*, 2022, **10**, 894252.
11 J.-m. Chen, Q.-y. Huang, Y.-x. Zhao, W.-h. Chen, S. Lin and Q.-y. Shi, *Front. Immunol.*, 2021, **12**, 785717.
12 X. Li, H. F. Lv, R. Zhao, M. f. Ying, A. T. Samuriwo and Y. Z. Zhao, *Mater. Today Bio*, 2021, **11**, 100101.
13 Y.-T. Song, P.-C. Liu, J. Tan, C.-Y. Zou, Q.-J. Li, J. Li-Ling and H.-Q. Xie, *Stem Cell Res. Ther.*, 2021, **12**(1), 556.
14 L. Xin, X. Zheng, J. Chen, S. Hu, Y. Luo, Q. Ge, X. Jin, L. Ma and S. Zhang, *Adv. Healthcare Mater.*, 2022, **11**(21), e2201680.
15 D. Lin-Cui, H. Yi-Zhou, X. Hui-Qi, Z. Bei-Hong, H. Yong-Can and D. Sheng-Rong, *Pharmaceutics*, 2021, **13**(11), 1796.
16 S. E. Moreno, M. Massee and T. J. Koob, *J. Biomed. Mater. Res., Part B*, 2022, **110**, 731–742.
17 R. Schwab and S. Reichl, *J. Mater. Sci.: Mater. Med.*, 2022, **33**(3), 29.
18 Q. Zhang, C. Chang, C. Qian, W. Xiao, H. Zhu, J. Guo, Z. Meng, W. Cui and Z. Ge, *Acta Biomater.*, 2021, **125**, 197–207.
19 N. Asadi, H. Pazoki-Toroudi, A. R. Del Bakhshayesh, A. Akbarzadeh, S. Davaran and N. Annabi, *Int. J. Biol. Macromol.*, 2021, **170**, 728–750.
20 X. Zhang, Z. Li, P. Yang, G. Duan, X. Liu, Z. Gu and Y. Li, *Mater. Horiz.*, 2021, **8**, 145–167.
21 X. Chen, J. Zhang, G. Chen, Y. Xue, J. Zhang, X. Liang, I. M. Lei, J. Lin, B. B. Xu and J. Liu, *Adv. Funct. Mater.*, 2022, **32**, 2202285.
22 X. Wang, X. Sun, D. Gan, M. Soubrier, H.-Y. Chiang, L. Yan, Y. Li, J. Li, S. Yu, Y. Xia, K. Wang, Q. Qin, X. Jiang, L. Han, T. Pan, C. Xie and X. Lu, *Matter*, 2022, **5**, 1204–1223.
23 M. Yang, Y. Zhang, C. Fang, L. Song, Y. Wang, L. Lu, R. Yang, Z. Bu, X. Liang, K. Zhang and Q. Fu, *Adv. Mater.*, 2022, **34**, 2109522.
24 H. Cao, L. Duan, Y. Zhang, J. Cao and K. Zhang, *Signal Transduction Targeted Ther.*, 2021, **6**, 426.
25 A. C. Madl, C. M. Madl and D. Myung, *ACS Macro Lett.*, 2020, **9**, 619–626.
26 L. Zhang, K. Yao, J. Wei, G. Li, Y. Lin, Y. L. Zhou and Y. Yang, *Appl. Mater. Today*, 2022, **27**, 101506.
27 Y. Xiong, X. Zhang, X. Ma, W. Wang, F. Yan, X. Zhao, X. Chu, W. Xu and C. Sun, *Polym. Chem.*, 2021, **12**, 3721–3739.
28 X. Chen, H. Yuk, J. Wu, C. S. Nabzdyk and X. Zhao, *Proc. Natl. Acad. Sci. U. S. A.*, 2020, **117**, 15497–15503.
29 J. Deng, H. Yuk, J. Wu, C. E. Varela, X. Chen, E. T. Roche, C. F. Guo and X. Zhao, *Nat. Mater.*, 2021, **20**, 229–236.
30 C. Wang, X. Chen, L. Wang, M. Makihata, H.-C. Liu, T. Zhou and X. Zhao, *Science*, 2022, **377**, 517–523.
31 Y. Jiang, G. Li, H. Wang, Q. Li and K. Tang, *Macromol. Biosci.*, 2022, **22**(5), e2100443.
32 J. Liang, Z. Guo, A. Timmerman, D. Grijpma and A. Poot, *Biomed. Mater.*, 2019, **14**(2), 024102.
33 H. Montazerian, A. Baidya, R. Haghniaz, E. Davoodi, S. Ahadian, N. Annabi, A. Khademhosseini and P. S. Weiss, *ACS Appl. Mater. Interfaces*, 2021, **13**, 40290–40301.
34 J. W. Yang, R. B. Bai, B. H. Chen and Z. G. Suo, *Adv. Funct. Mater.*, 2020, **30**, 1901693.
35 M. S. Desai, M. Chen, F. H. J. Hong, J. H. Lee, Y. Wu and S.-W. Lee, *Biomacromolecules*, 2020, **21**, 2938–2948.
36 Y. Liu, K. Ai and L. Lu, *Chem. Rev.*, 2014, **114**, 5057–5115.
37 Y. C. Zhang, Q. Chen, Z. W. Dai, Y. Dai, F. Xia and X. J. Zhang, *J. Mater. Chem. B*, 2021, **9**, 585–593.
38 D. Gan, W. Xing, L. Jiang, J. Fang, C. Zhao, F. Ren, L. Fang, K. Wang and X. Lu, *Nat. Commun.*, 2019, **10**, 1487.
39 M. H. Kim, J. Lee, J. N. Lee, H. Lee and W. H. Park, *Acta Biomater.*, 2021, **123**, 254–262.
40 P. K. Forooshani and B. P. Lee, *J. Polym. Sci., Part A: Polym. Chem.*, 2017, **55**, 9–33.
41 M. Pan, K.-C. T. Nguyen, W. Yang, X. Liu, X.-Z. Chen, P. W. Major, L. H. Le and H. Zeng, *Chem. Eng. J.*, 2022, **434**, 134418.
42 Z. Yang, R. Huang, B. Zheng, W. Guo, C. Li, W. He, Y. Wei, Y. Du, H. Wang, D. Wu and H. Wang, *Adv. Sci.*, 2021, **8**, 2003627.
43 Z. Guo, Z. Zhang, N. Zhang, W. Gao, J. Li, Y. Pu, B. He and J. Xie, *Bioact. Mater.*, 2022, **15**, 203–213.
44 C. Mao, Y. Xiang, X. Liu, Y. Zheng, K. W. K. Yeung, Z. Cui, X. Yang, Z. Li, Y. Liang, S. Zhu and S. Wu, *ACS Appl. Mater. Interfaces*, 2019, **11**, 17902–17914.
45 W. Zhang, R. Wang, Z. Sun, X. Zhu, Q. Zhao, T. Zhang, A. Cholewinski, F. Yang, B. Zhao, R. Pinnaratip, P. K. Forooshani and B. P. Lee, *Chem. Soc. Rev.*, 2020, **49**, 433–464.
46 L. Han, L. Yan, K. Wang, L. Fang, H. Zhang, Y. Tang, Y. Ding, L.-T. Weng, J. Xu, J. Weng, Y. Liu, F. Ren and X. Lu, *NPG Asia Mater.*, 2017, **9**, e372.
47 J. Yang, R. Bai, B. Chen and Z. Suo, *Adv. Funct. Mater.*, 2020, **30**, 1901693.
48 X. Fan, Y. Fang, W. Zhou, L. Yan, Y. Xu, H. Zhu and H. Liu, *Mater. Horiz.*, 2021, **8**, 997–1007.
49 Y. Yi, C. Xie, J. Liu, Y. Zheng, J. Wang and X. Lu, *J. Mater. Chem. B*, 2021, **9**, 8739–8767.
50 Y. Zhao, S. Song, X. Ren, J. Zhang, Q. Lin and Y. Zhao, *Chem. Rev.*, 2022, **122**, 5604–5640.
51 C. Cui, T. Wu, X. Chen, Y. Liu, Y. Li, Z. Xu, C. Fan and W. Liu, *Adv. Funct. Mater.*, 2020, **30**, 2005689.
52 D. H.-K. Ma, J.-Y. Lai, H.-Y. Cheng, C.-C. Tsai and L.-K. Yeh, *Biomaterials*, 2010, **31**, 6647–6658.
53 S. Cavalu, G. Roiu, O. Pop, D. A. P. Heredea, T. O. Costea and C. F. Costea, *Materials*, 2021, **14**, 863.

54 J. H. Arrizabalaga and M. U. Nollert, *ACS Biomater. Sci. Eng.*, 2018, **4**, 2226–2236.
55 M. Litwiniuk and T. Grzela, *Wound Repair Regen*, 2014, **22**, 451–456.
56 H. Lv, B. Wu, J. Song, W. Wu, W. Cai and J. Xu, *J. Mater. Chem. B*, 2021, **9**, 6536–6552.
57 H. Elkhenany, A. El-Derby, M. Abd Elkodous, R. A. Salah, A. Lotfy and N. El-Badri, *Stem Cell Res. Ther.*, 2022, **13**, 8.
58 H. Zhou, S. Li, H. Liu, B. Zheng, X. Jin, A. Ma and W. Chen, *Macromol. Mater. Eng.*, 2020, **305**, 1900621.
59 C. T. Koh, K. Tonsomboon and M. L. Oyen, *Interface Focus*, 2019, **9**, 20190012.